Annual Review of Analytical Chemistry

Real-Time Visualization and Monitoring of Physiological Dynamics by Aggregation-Induced Emission Luminogens (AIEgens)

Xuewen He,[1,2,3] Jacky W.Y. Lam,[1,3] Ryan T.K. Kwok,[1,3] and Ben Zhong Tang[1,2,3,4,5]

[1]Department of Chemistry, The Hong Kong Branch of Chinese National Engineering Research Centre for Tissue Restoration and Reconstruction, Institute for Advanced Study, Division of Life Science and State Key Laboratory of Molecular Neuroscience, The Hong Kong University of Science and Technology, Clear Water Bay, Kowloon, Hong Kong 999077, China; email: chryan@ust.hk, tangbenz@ust.hk

[2]Department of Chemical and Biological Engineering, The Hong Kong University of Science and Technology, Clear Water Bay, Kowloon, Hong Kong 999077, China

[3]HKUST-Shenzhen Research Institute, Shenzhen 518057, China

[4]Center for Aggregation-Induced Emission, SCUT-HKUST Joint Research Laboratory, State Key Laboratory of Luminescent Materials and Devices, South China University of Technology, Guangzhou 510640, China

[5]AIE Institute, Guangzhou Development Distinct, Huangpu, Guangzhou 516530, China

Keywords

aggregation-induced emission, real-time, physiological dynamics, fluorescence, bioprobe

Abstract

Physiological dynamics in living cells and tissues are crucial for maintenance and regulation of their normal activities and functionalities. Tiny fluctuations in physiological microenvironments can leverage significant influences on cell growth, metabolism, differentiation, and apoptosis as well as disease evolution. Fluorescence imaging based on aggregation-induced emission luminogens (AIEgens) exhibits superior advantages in real-time sensing and monitoring of the physiological dynamics in living systems, including its unique properties such as high sensitivity and rapid response, flexible molecular design, and versatile nano- to mesostructural fabrication. The introduction of canonic AIEgens with long-wavelength, near-infrared, or microwave emission, persistent luminescence, and diversified excitation source (e.g., chemo- or bioluminescence) offers researchers a tool to evaluate the resulting molecules with excellent performance in response to subtle fluctuations in bioactivities with broader dimensionalities and deeper hierarchies.

1. INTRODUCTION

Physiological microenvironments are essential for living organisms to stay alive and perform normal functions. Dynamics in physiological microenvironments can have significant influence on such issues as enzymatic activity, metabolic rate, and gene expression level and, in turn, shape the adaptive responsiveness to environmental stimuli. Studies have increasingly shown that the abnormal fluctuations in physiological dynamics facilitate the occurrence and development of various diseases (1–3). For example, different from that in normal tissues, the physiological environment in tumoral tissues is unique and includes hypoxia, acidic extracellular pH, and tolerance to oxidation stress. These heterogenized microenvironments not only differentiate the tumors from the normal tissues but also promote oncogenesis with inextricable linkages (1). Therefore, real-time monitoring of physiological dynamics in living systems is of great importance to reveal the initiation and evolution mechanisms of diseases and to precisely diagnose and treat diseases for improved health.

The past few decades have witnessed remarkable progress in bioimaging techniques that form the basis of life science research and biomedical diagnosis. Various types of tools, including computed tomography, ultrasound, magnetic resonance imaging, positron emission tomography, and cryo-electron microscopy, have been developed so that the biostructures at the tissue or even cellular level could be visualized with high sensitivity, high spatial-temporal resolution, and deep penetrability (4, 5). Among them, fluorescence imaging possesses unique advantages for in situ visualization of biotargets at the molecular level and monitoring dynamic biological processes in real time (6–9). However, traditional organic fluorophores with large plane π-conjugation exhibit several drawbacks, such as severe photobleaching, moderate signal-to-noise ratio, and aggregation-caused quenching (ACQ). Although inorganic quantum dots and upconverting nanoparticles show bright luminescence and excellent photostability (10–12), their heavy metal components present toxicity concerns that limit their further clinical translations (13, 14).

Unlike the ACQ fluorophores, aggregation-induced emission luminogens (AIEgens) represent superior alternatives for fluorescence light-up imaging. The rotor-containing AIEgens undergo low-frequency motions when they are well dissolved in good solvents. This molecular motion dissipates the exciton energy through fast nonradiative pathways to contribute to the nonemissive nature of molecules in the solution state. While in the aggregated form, strong emission was observed due to the restriction of intramolecular motion to block the nonradiative decay channels (15, 16). Owing to their large Stokes shifts, strong photobleaching resistance, and excellent biocompatibility, AIE-based materials have been widely applied in the visualization of biomolecules and structures among various hierarchies and dimensionalities, including specific biomolecule analysis (17, 18), real-time subcellular or cellular imaging (19, 20), high-resolution tissue visualization (21), and precise whole-body monitoring (22). Importantly, AIEgens are also utilized for investigating complex bioprocesses such as drug delivery (23), short interfering RNA (siRNA)/gene interference (24, 25), bacteriophage infection (26), and cancer therapy (27, 28), thanks to their ultrahigh sensitivity, rapid responsiveness, and superior temporal resolution. In this review, we focus on monitoring of physiological dynamics in intracellular pH, temperature, microviscosity and polarity, membrane potential, hypoxia, redox balance, and radicals to provide insightful information to evaluate cellular dysfunctionality and the evolution of disease (**Figure 1**).

2. INTRACELLULAR pH MONITORING

Intracellular pH is an essential factor that regulates various cellular behaviors (29). Abnormal intracellular pH is a hallmark of many diseases (30). Sensing and monitoring of pH changes inside living cells are thus of great importance for gaining insights into their pathological processes.
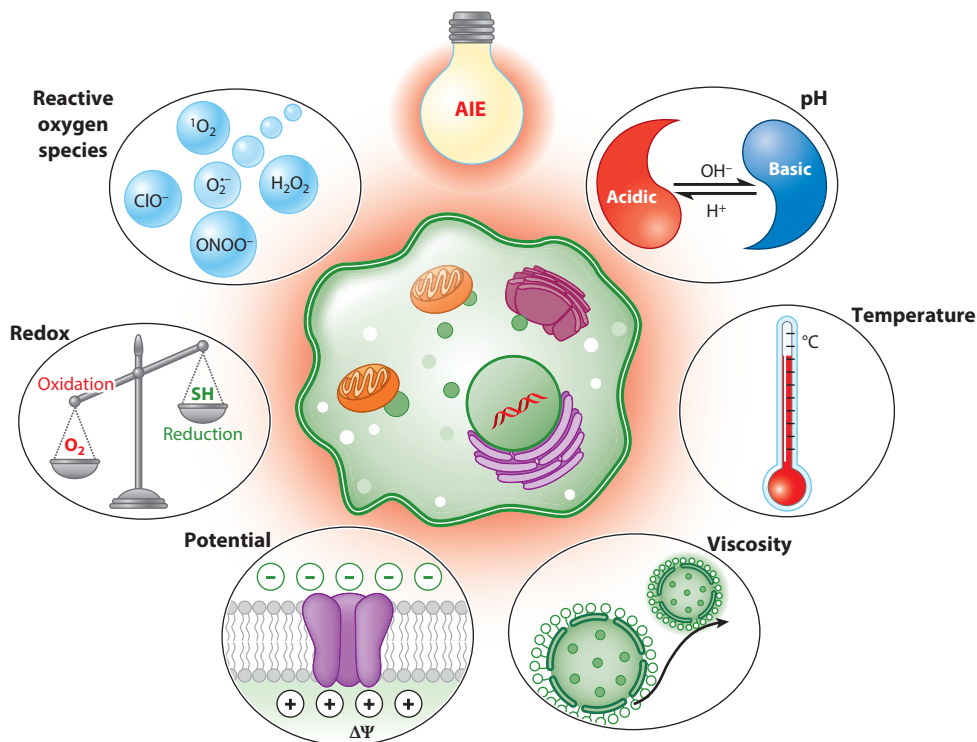
Figure 1

Aggregation-induced emission (AIE) luminogens lighting up the physiological environment in living cells through fluorescence imaging of the intracellular dynamics in pH, temperature, viscosity, potential, redox, reactive oxygen species, and other factors.

2.1. Small-Molecule-Based Intracellular pH Sensors

Tang's group (31) reported a full-range pH response probe, tetraphenylethene-cyanine (TPE-Cy) adduct, with a sulfonic group and cyanine as active sites toward H^+ and OH^-, respectively. TPE-Cy showed strong-to-medium red emission at pH 5.0−7.0, weak-to-nil red emission at pH 7.0−10, and nil-to-strong blue emission at pH 10−14, with the conjugation structure broken down (**Figure 2a**). Cytoplasmic pH sensing and quantitation were thus realized via a ratiometric manner. In particular, upon acid treatment, the pseudo red-color-stained area greatly expanded. When the acid was replaced by Dulbecco's Modified Eagle Medium (DMEM, pH 8.5), blue color dominated the regions, indicating sensitive responses to pH changes (31). Similar strategies using pyridines (32, 33), Schiff bases (34), benzimidazole (35), tertiary amines (36), quinoline (37), and phenol (38) as proton/base reactive groups were also applied in intracellular pH monitoring.

In situ monitoring of pH at the subcellular level was also realized by functionalizing the probes with specific organelle-targeting groups. Xi and coworkers (39) developed a near-infrared (NIR) probe by incorporating a TPE unit with a NIR merocyanine skeleton whose positive charge could guide the probe accumulated on the mitochondrial membrane. The hydroxyl xanthene unit enabled a sensitive fluorescence response to the local pH dynamics, with a high tolerance to membrane potential change (39). Similarly, by specific modification of acid responsive moieties, e.g., morpholine groups, the monitoring of pH dynamics in lysosomes was also conducted to evaluate the cells' functionality (40, 41).
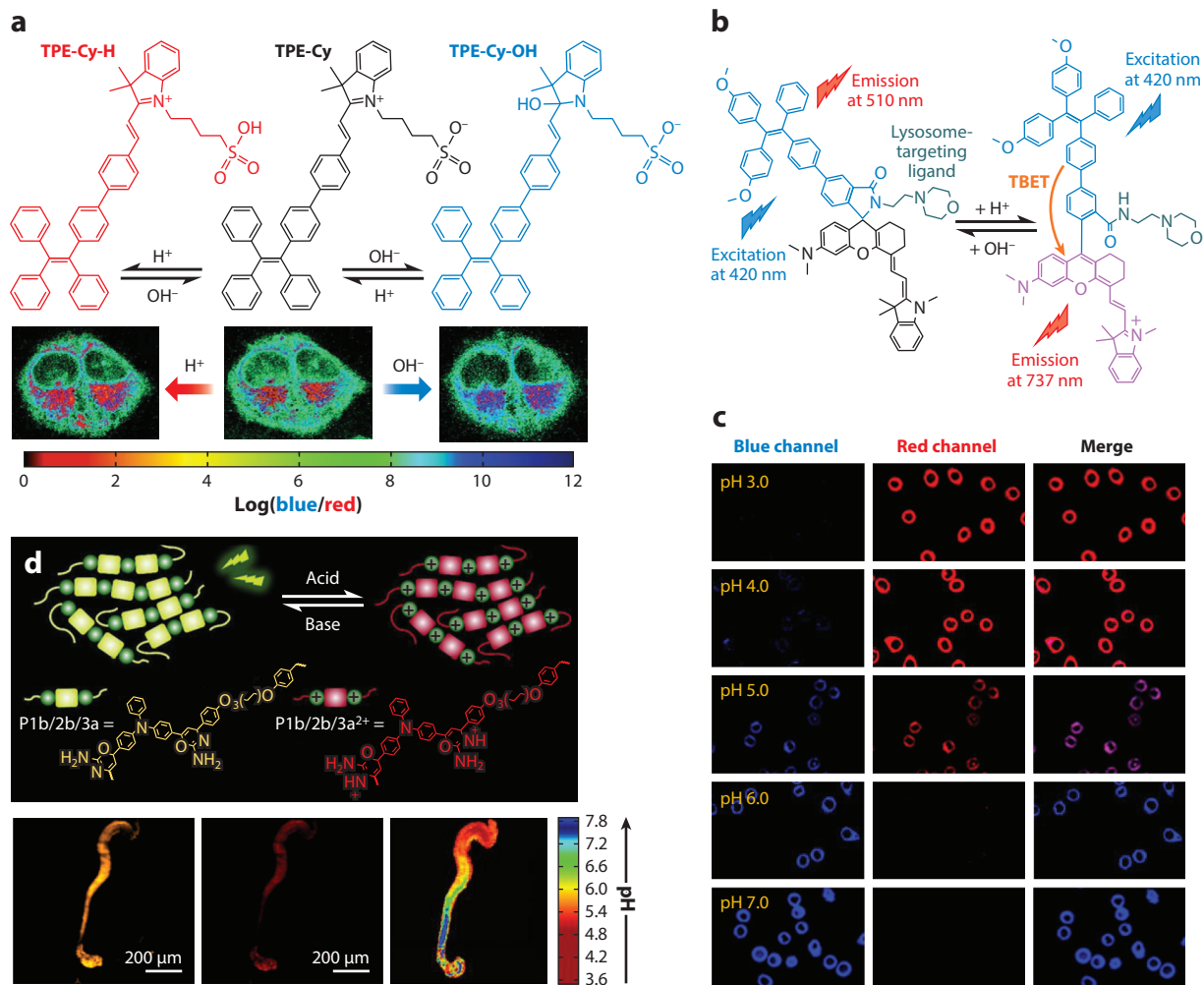
Figure 2

pH sensing in living systems. (*a*) Working principle for the fluorescent response of TPE-Cy to pH change. Panel adapted with permission from Reference 31; copyright 2013 American Chemical Society. (*b*) Chemical responses of a ratiometric AIE-TBET probe to pH changes by emitting various emission colors. (*c*) Fluorescence images of HeLa cells incubated with probe in panel *b*, with pH changing from 3.0 to 7.0. Panels *b–c* adapted with permission from Reference 44; copyright 2018 American Chemical Society. (*d, top*) Scheme of acid- and amine-responsive mechanisms by protonation of P1b/2b/3a and deprotonation of P1b/2b/3a^{2+}. (*d, bottom*) From left to right: After incubation with P1b/2b/3a, the confocal images of *Moina macrocopa* are shown with orange and red emissions and calculated pH heat images, respectively. Panel adapted with permission from Reference 46; copyright 2019 Wiley-VCH Verlag. Abbreviations: AIE, aggregation-induced emission; TBET, through-bond energy transfer; TPE-Cy, tetraphenylethene-cyanine.

Förster resonance energy transfer (FRET) was widely employed to achieve large Stokes shifts that were highly desired for accurate sensing. For instance, Yang's group (42) developed a sensor combining AIE and FRET with Stokes shifts as large as 138 nm between the excitation and emission from cyano-diphenylethylene and BODIPY, respectively. With a pK_a value of 9.79, it sensitively responded to pH 9.0−10 in living cells. The strict requirement of well overlapping between the donor's emission and acceptor's absorbance in FRET pairs could be further re-solved by through-bond energy transfer (TBET) (43). For example, Wang et al. (44) developed

a TBET probe composed of a TPE donor and an NIR hemicyanine acceptor. As shown in **Figure 2b**, the probe showed strong blue fluorescence at neutral or basic pH with closed hemicyanine. When pH decreased from 7.0 to 3.0, the TBET effect was activated with a 238-fold enhancement in the ratio of NIR fluorescence to blue fluorescence. Moreover, well-separated dual emissions with a pseudo-Stokes shift up to 361 nm were realized, facilitating precise double-checked imaging of cellular pH fluctuation (44) (**Figure 2c**).

2.2. Polymers

In addition, AIE-based polymers represent excellent alternatives in pH sensing with their even broader detection range and higher signal amplification factor owing to their capability to interact with multiple protons. Tian's group (45) designed an amphiphilic copolymer containing TPE-oxazolidine as a pH-sensitive chromophore and a polyethylene glycol (PEG) derivative as a water-soluble chain. In an acidic lysosome, the probe changed from cyan to red due to intramolecular charge transfer (ICT) effect of opening the spiro-ring of oxazolidine moiety. The probe emission was then switched back to cyan from red in response to lysosomal inhibitors, enabling real-time monitoring of pH-related autophagy in cancer cells (45). Expanding into in vivo pH mapping, Tang's group (46) developed a multifunctional polymer [poly(2-amino-4*H*-1,3-oxazine)s] (PAHOs) with *N*-heterocycles for pH sensing. As shown in **Figure 2d**, PAHOs displayed ratiometric sensing behavior within a broad pH window from 1.0 to 9.0 by emitting yellow to red fluorescence accordingly. Intestinal pH in *Moina macrocopa* was then mapped as pH gradually increased from 4.2 to 7.8 along the digestive process in its intestinal lumen, consistent with its biological nature (46).

3. INTRACELLULAR TEMPERATURE SENSING

Temperature is critical for cells because it regulates every intracellular biochemical reaction (47). Sensing the intracellular temperature, especially in inflammatory and tumor cells, can provide valuable insights into their pathology and physiology.

Thermo-responsible AIE materials have been widely applied in temperature sensing. Chen's group (48) designed a fluorescence lifetime–based thermometer using AIE-active hexaphenylsilole (HPS) as the reporter and butter as the matrix (**Figure 3a**). The viscosity of the matrix decreased when the butter melted under increased temperature. Thus, the intramolecular motion of HPS was accelerated in response to fluorescence lifetime. Shorter fluorescence lifetime upon increased temperature was observed with a resolution up to ∼0.11 ns/°C. Because it was encapsulated inside, the signal from the reporter was highly specific to the temperature change without interference from pH or ionic strength. As shown in **Figure 3b**, the fluorescence lifetime was 1.45 ns at 24°C, whereas it was only 0.83 ns at 38°C in living cells (48).

Another strategy based on thermoresponsive emission color change was employed by Wang et al. (49) for intracellular temperature sensing (**Figure 3c**). Blue AIE cages were used as initiators to synthesize amphipathic star-like poly(*N*-isopropylacrylamide) (PNIPAM) polymer that can self-assemble into nanoparticles. The PNIPAM either shrank or extended according to temperature, with characteristic lower critical solution temperature at 32°C. Therefore, the sensor could be easily tuned to various color emissions through a cascade FRET effect after encapsulating different doses of guest dyes [(4-dimethylamino-2′-butoxychalcone (DMBC) and Nile red with yellow and red emission, respectively]. Moreover, the white emissive polymeric nanoparticles exhibited a reversible response to temperature with a resolution of about 0.5°C. As shown in **Figure 3d**, with temperature increasing from 25°C to 45°C, the fluorescence intensity between 450 nm and 530 nm decreased but increased at 620 nm, resulting in the shift of fluorescence emission color from red to white. This multicolor thermometer represented an excellent alternative to report inhomogeneous physiological parameters in different cells, tissues, and organs (49).
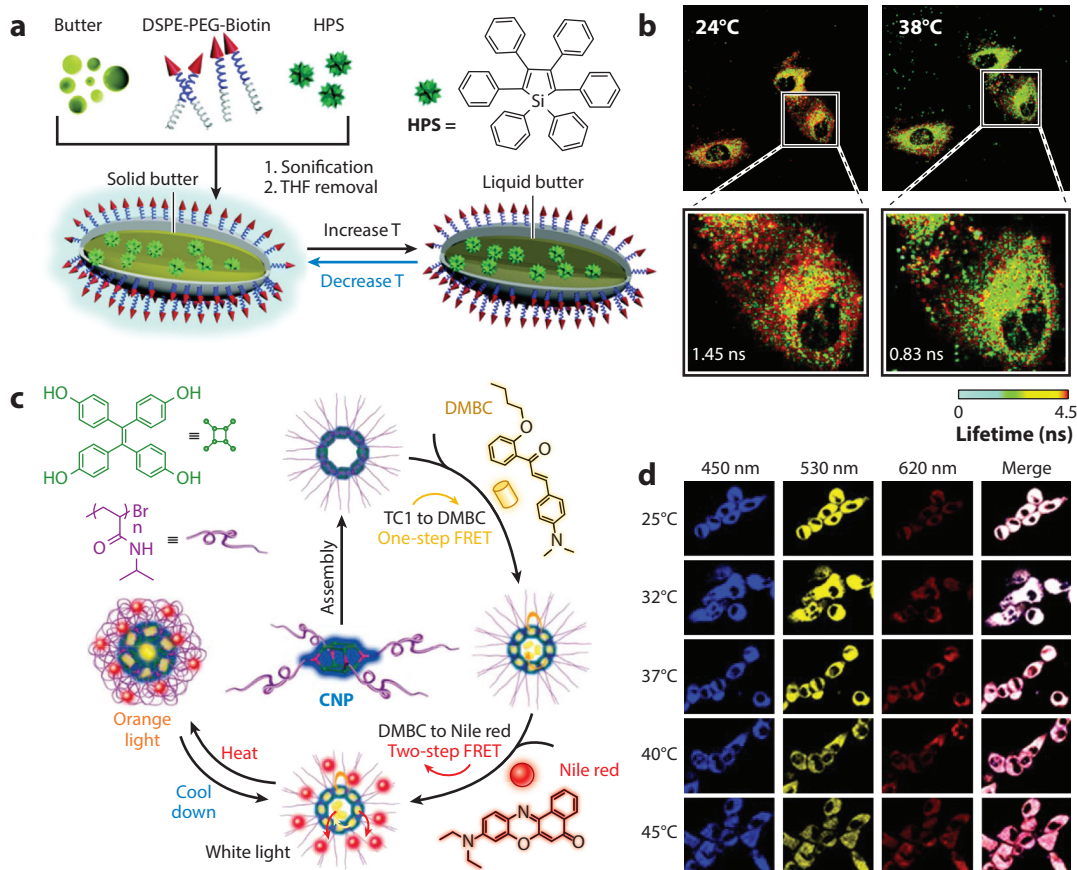
Figure 3

Temperature sensing in living cells. (*a*) Schematic diagram of the synthetic process of the HPS/butter/DSPE-PEG-biotin nanorod. Alterations of the position of HPS molecules and the orientation of the DSPE-PEG-biotin segment are not shown and the size of the nanorod is not drawn to scale. (*b*) In vitro fluorescence lifetime images and the corresponding fluorescence decay curves of the HPS/butter/DSPE-PEG-biotin nanorod in live cells measured at indicated temperatures. Panels *a–b* adapted with permission from Reference 48; copyright 2020 Royal Society of Chemistry. (*c*) Graphical representation of CNP assembly into hybrid nanoparticles and the temperature-sensing profiles with varying emission colors. (*d*) Confocal images of HeLa cells stained with white light–emitting hybrid nanoparticles at different temperatures. Panels *c–d* adapted with permission from Reference 49; copyright 2020 American Chemical Society. Abbreviations: CNP, cage-based poly(*N*-isopropylacrylamide) polymer; DMBC, 4-dimethylamino-2′-butoxychalcone; DSPE-PEG-biotin, 1,2-distearoyl-*sn*-glycero-3-phosphoethanolamine-*N*-(biotinyl-PEG-2000)-biotin; FRET, Förster resonance energy transfer; HPS, hexaphenylsilole; PEG, polyethylene glycol; T, temperature; THF, tetrahydrofuran.

4. VISCOSITY AND POLARITY MONITORING

Intracellular viscosity is a crucial parameter that determines the rate of diffusion-controlled processes in living systems (50). The abnormality of intracellular viscosity has been regarded as an indicator of various diseases (51). By coincidence, AIEgens with rotors that are sensitive to viscosity have been widely applied in monitoring intracellular viscosity.

Tang's group (52) used the abovementioned TPE-Cy for microviscosity sensing because of its rotor-like structure and excellent permeability and biocompatibility. Longer fluorescence lifetime was observed in higher-viscous solution and a more tightly packed membrane environment. Two-photon fluorescence lifetime imaging in living cells revealed that lipid droplets possessed

much lower viscosity than the surrounding cytoplasmic area, with lifetime values ranging from a few hundred picoseconds to more than 1.5 ns, thereby providing an excellent tool for related applications (52). Owing to the heterogenic nature of intracellular viscosity, it is essential to develop organelle-specific probes for in situ viscosity monitoring. Jiang's group (53) reported a pyridinium-modified water-soluble viscometer probe, MitoAIE1, that could specifically target the mitochondria (**Supplemental Figure 1a,b**). With viscosity increasing from 0.894 cP [poly (butylene succinate) (PBS)] to 942.5 cP (99% glycerol), the fluorescence intensity of MitoAIE1 increased by 38-fold, indicating sensitive responses to viscosity (53).

A microenvironmental factor, polarity, could also have a significant influence on intracellular biomolecular diffusion and membrane trafficking (54). To quantify the subcellular polarity change in response to protein unfolding, Wong and colleagues (55) reported an AIE probe, NTPAN-MI, whose fluorescence could be selectively activated upon labeling exposed thiols in unfolded proteins by interrupting the photoinduced electron transfer (PET) effect. As shown in **Supplemental Figure 1c,d**, the fluorescence emission wavelength of NTPAN-MI was red shifted with increasing solvent polarity. Through spectral phasor analysis, distinct patterns of dielectric constant distribution in the cytoplasm can be observed before and after MG132 stimulation that could disrupt the normal protein degradation pathways. In particular, in the nucleus, the unfolded proteome experienced the most hydrophilic environment compared to that in the endoplasmic reticulum and cytosol area, indicating a sensitive response to the subcellular polarity dynamics of living cells during the antistress process (55).

5. MEMBRANE POTENTIAL SENSING

Membrane potential originates from the voltage difference between the inside and outside of a cell or subcellular organelle. Changes in membrane potential can elicit action potentials in neuron cells and affect the cellular respiration for generating energy on the mitochondrial membrane (56, 57).

By introducing a mitochondrion targeting group, triphenylphosphonium (TPP), Yoon's group (58) prepared an AIE probe, TPE-ca-TPP (**Supplemental Figure 2a**) to monitor local potential changes ($\Delta\psi_m$). The positive-charge TPP subunit can guide the AIE probe to selectively accumulate on the mitochondria because of their negative potential gradient, with a strong emission of green fluorescence. In contrast, after treatment with an oxidative inhibitor that could neutralize the mitochondrial membrane potential, the fluorescence signal from the probe almost disappeared, indicating its sensitive response to $\Delta\psi_m$ (58).

Because the mitochondria can provide energy for sperm movement, the abnormal $\Delta\psi_m$ may lead to dysfunction in male infertility. Tang's group (59) and Jiang's group (60) independently demonstrated two kinds of AIEgens conjugated with cationic indolium groups, TPE-In and TPE-Ph-In, that could perfectly target mitochondria in mammalian sperm cells. Both are AIE-active and emit in the red region in their aggregate state with a Stokes shift larger than 200 nm. Gu and colleagues (61) further utilized TPE-Ph-In to evaluate the quality of human sperm cells via imaging of mitochondrial membrane potential. Taking advantage of this high-throughput method, investigators stained clinical sperm samples from 36 infertile patients with TPE-Ph-In. As shown in **Supplemental Figure 2b**, a positive correlation was constructed between the motility of four grades of sperm cells and their mitochondrial membrane potentials, enabling early diagnosis of male fertilization conditions (61).

Cationic pyridinium served as another alternative for mitochondrion targeting. Tang's group (62) reported an azide-functionalized tetraphenylethene pyridinium (TPE-Py-N$_3$) probe. As shown in **Supplemental Figure 2c**, the excellent membrane penetrability of TPE-Py-N$_3$ probes

allowed them to diffuse into all cells within the zebrafish embryos by showing a robust fluorescence signal. It became almost negligible after staurosporine (an apoptosis-inducing chemical) treatment, leaving only weak autofluorescence (62).

6. HYPOXIA DETECTION IN LIVING CELLS AND TISSUES

Hypoxia caused by the lack of oxygen is associated with a variety of conditions such as cardiac ischemia, stroke, and inflammation. In particular, as an important characteristic of solid tumors, hypoxia is directly related to tumor progression, metastasis, and drug resistance (1).

Azoreductase, which is overexpressed in hypoxic tumor sites, can efficiently reduce the N=N bond through a two-electron transfer process. Taking advantage of the macromolecular azo coupling reaction between a PEG diazonium salt and a TPE-modified aniline, He and coworkers (63) constructed a relevant probe, PEG-Azo-TPE. As shown in **Figure 4*a***, micelles could be formed in aqueous solution to yield azobenzene-caged AIE dots. Their sensitive responses to hypoxia were verified by the lit-up fluorescence signals in cancer cells after transferring to hypoxia (1% O_2) from normoxia (20% O_2) (63). Recently, in situ hypoxia imaging was performed using water-soluble azobenzene-contained copolymer (WS-AC) and anionic water-soluble tetraphenylethene (AWS-TPE). Imaging showed a very weak fluorescence signal because of its good water solubility. When the azobenzene moiety was cleaved by the overexpressed azoreductases, WS-AC transformed into a cationic species, which could further assemble in situ with the opposite-charge AWS-TPE. As a result, the AIE was activated with an intensified fluorescence signal to illuminate the hypoxia in the multicellular tumor spheroid model (64).

With the aid of *N*-oxides, a new strategy was reported by Tang's group (65) for hypoxia imaging. The as-prepared TPE-2E *N*-oxide dispersed well in an aqueous medium, leading to a negligible fluorescence signal. Cytochrome P450s existing in the hypoxic tumor can catalyze a two-electron reduction of *N*-oxides. As shown in **Figure 4*b***, along with the decrease in oxygen density from 21% to 0% in HeLa cells, TPE-2E *N*-oxide showed a gradually intensified fluorescence signal, confirming its sensitivity to hypoxia (65). Studies indicated that the activity of nitroreductase is closely related to hypoxia in living cells and tissues. Zhang's group (66) thus explored a molecule, TPE-NO$_2$, for tumor hypoxia imaging by endowing the TPE unit with a nitro group. Upon treatment with nitroreductase and NADH, pyridine-substituted TPE (TPE-PY) was produced, leading to the transformation from hydrophilic to hydrophobic. The resulting aggregation of TPE-PY generated a 55-fold turn-on intensity in fluorescence signal, showing an excellent sensitivity to hypoxic cancer cells. By combining fluorescence and photoacoustic signals, Wu and coworkers (67) further designed a squaraine-based dual-modality AIEgen for in vivo hypoxia imaging. As shown in **Figure 4*c***, the probe was readily assembled into a nanoparticle (SPT-NO$_2$) in aqueous media owing to its amphiphilicity. The presence of nitroreductase converted the electron-withdrawing nitro group into an electron-donating amino group, leading to a 52-nm blue shift in absorption peak and apparent enhancements in fluorescence signal. Therefore, strong photoacoustic and fluorescence signals were observed in the tumor site, providing clear information about the hypoxic status in living animals (**Figure 4*d***) (67).

7. REDOX BALANCE MONITORING

Biothiols, including cysteine (Cys), homocysteine (Hcy), glutathione (GSH), and hydrogen sulfide (H$_2$S), are essential in cell signaling, growth, and apoptosis (68). Moreover, biothiols have strong redox properties and nucleophilicity and serve as key antioxidants to counter endogenous reactive oxygen species (ROS) and other free radicals (2).
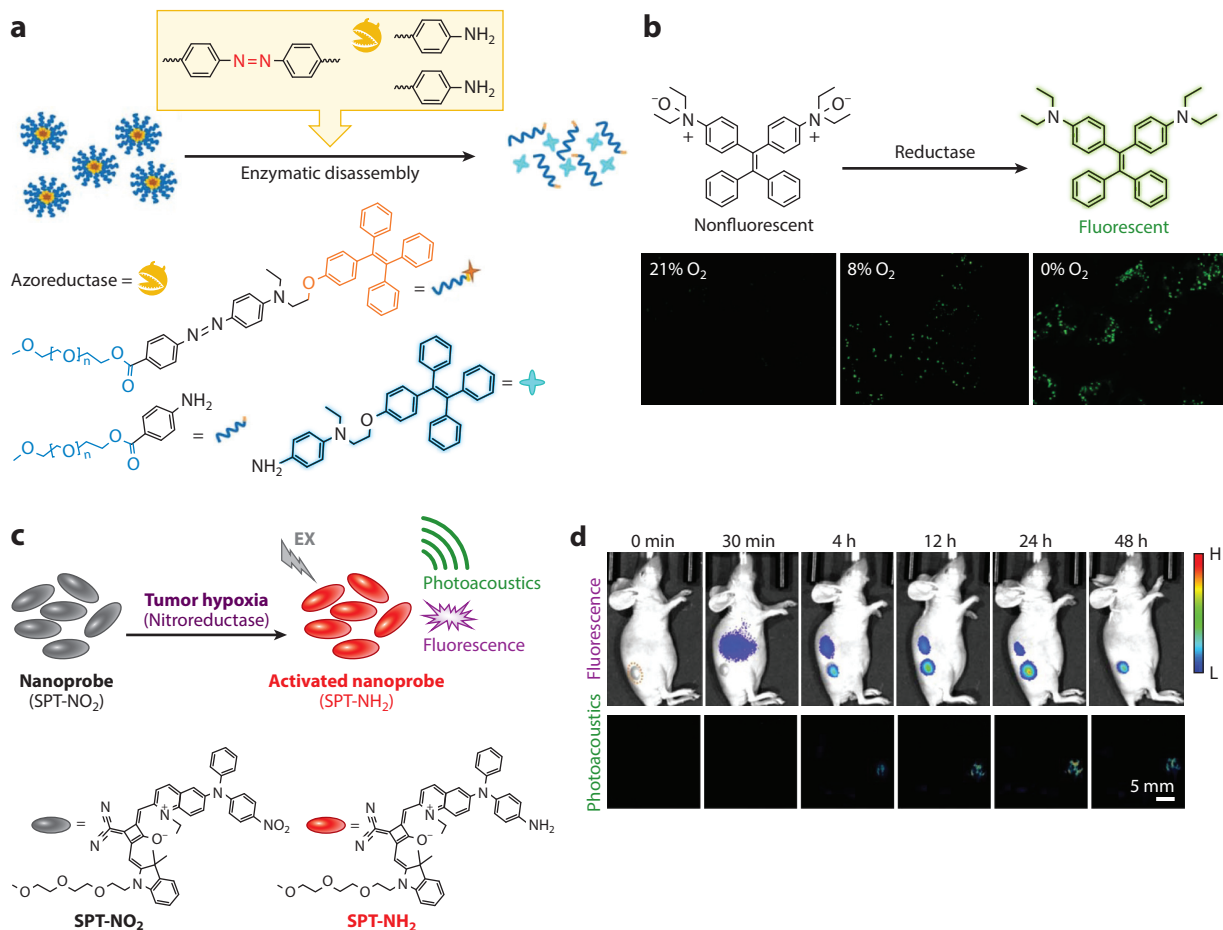
Figure 4

Hypoxia sensing in living systems. (*a*) Scheme for sensing of hypoxia-induced azoreductase by polymeric aggregation-induced emission (AIE) aggregates. Panel adapted with permission from Reference 63; copyright 2019 Wiley-VCH Verlag. (*b*, *top*) Scheme of hypoxia detection based on the hydrophilic to hydrophobic transition of TPE-2E *N*-oxide to TPE-2E catalyzed by intracellular reductases. (*b*, *bottom*) Fluorescent images of HeLa cells cultured with TPE-2E *N*-oxide under various oxygen concentrations. Panel adapted with permission from Reference 65; copyright 2019 Wiley-VCH Verlag. (*c*) Scheme of the nanoprobe's response toward nitroreductase under tumor hypoxia by generating ultrasound and fluorescence signals. (*d*) Fluorescence and ultrasound imaging of mice bearing subcutaneous tumors at various times upon injection of the nanoprobes. Panels *c–d* adapted with permission from Reference 67; copyright 2019 Wiley-VCH Verlag.

7.1. Cys and Hcy Monitoring

Among those biothiols, Cys and Hcy are not only involved in protein and peptide structure, but they also regulate biological nitrogen balance and redox homeostasis. The deficiency of Cys can lead to growth retardation in children, hair depigmentation, liver damage, and muscle loss, whereas an elevated level of Cys could cause cardiovascular disease and neurotoxicity (68).

By utilizing the PET effect, Tang and coworkers (69) reported a powerful turn-on thiol-specific probe, TPE-MI (**Figure 5a**, **subpanel i**). The maleimide (MI) group served as a specifically recognizing thiol group. It can efficiently quench the fluorescence signal of the TPE core in both solution and aggregate states, due to the exciton annihilation process associated with the *n*-π
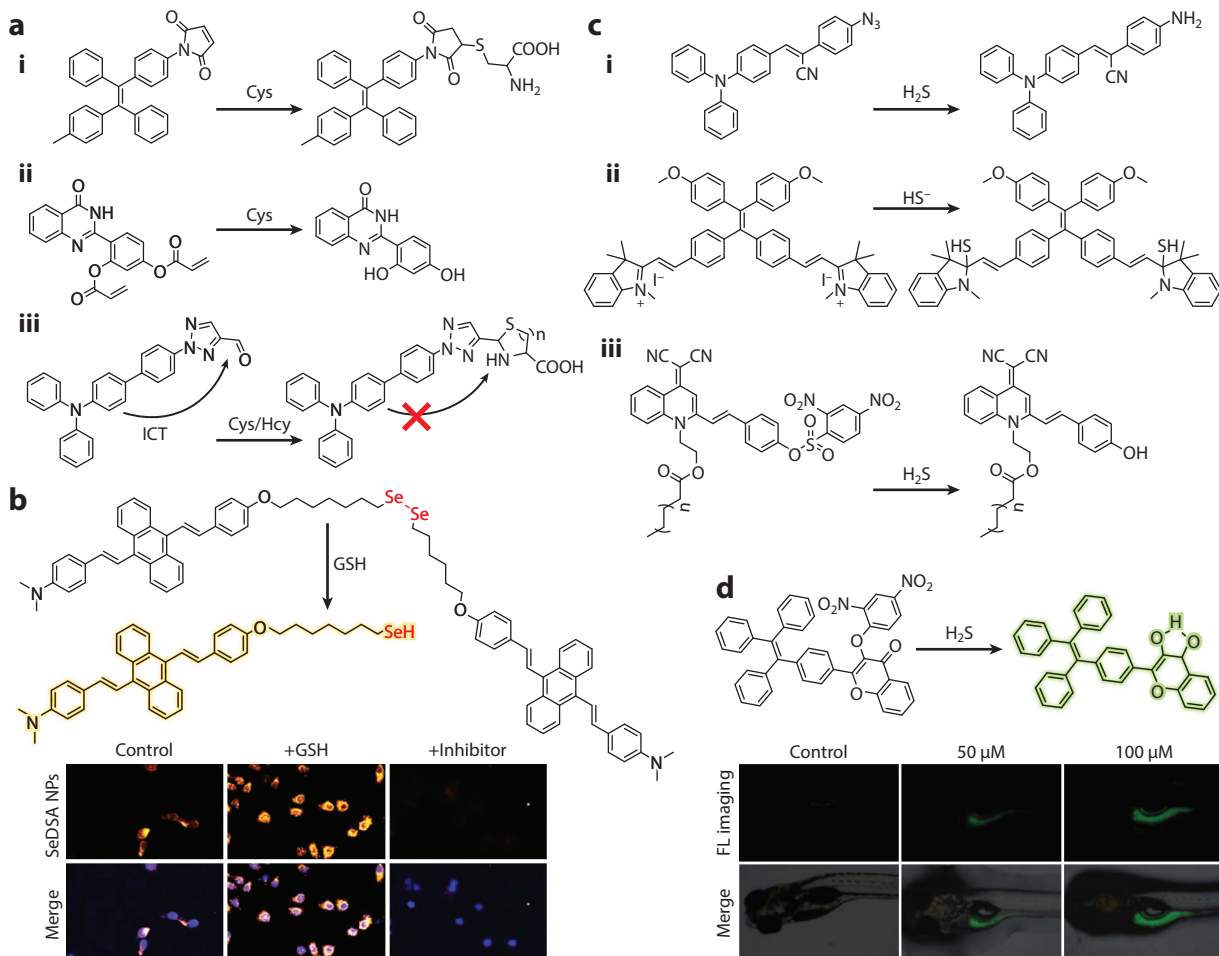
Figure 5

Redox balance sensing in living systems. (*a*) Representative strategies for thiol-containing amino acid detection. (*b, top*) Representative reaction for GSH detection via reduction of the Se-Se bond in SeDSA NPs. (*b, bottom*) Confocal images of HepG2 cells incubated with SeDSA NPs after treatment with GSH and NEM inhibitors with cell nuclei (*blue*) and SeDSA NPs (*orange*). Panel adapted with permission from Reference 78; copyright 2019 Wiley-VCH Verlag. (*c*) Representative strategies for H$_2$S detection. (*d, top*) One representative strategy for H$_2$S imaging in living cells. (*d, bottom*) Fluorescent images of zebrafish larvae pretreated with the nanoprobe (the control) and then incubated with 50 mM and 100 mM H$_2$S. Panel adapted with permission from Reference 86; copyright 2017 Royal Society of Chemistry. Abbreviations: Cys, cysteine; FL, fluorescence; GSH, glutathione; H$_2$S, hydrogen sulfide; Hcy, homocysteine; HepG2, human liver cancer cell line; ICT, intramolecular charge transfer; NEM, *N*-ethylmaleimide; NP, nanoparticle; SeDSA, diselenide-containing 9,10-distyrylanthracene derivative.

electronic conjugation of the carbonyl (C=O) and olefinic (C=C) groups. When the thiol group conjugated onto the C=C bond in the MI moiety by thiol-ene hydrothiolation reaction, the *n*-π conjugation was broken down and the PET effect of MI on TPE was interrupted. As a result, a lit-up fluorescence signal could be achieved in the range of 1 to 100 ng/mL, which is a promising result for intracellular Cys sensing (69).

Another strategy of introducing the excited-state intramolecular proton transfer (ESIPT) effect into AIEgen was reported by Jiang's group (70) for Cys detection in living cells. The

intramolecular cyclization between acrylate and Cys broke the acryloyl group in the probe, activating the ESIPT process by emitting a strong fluorescence signal. Superior selectivity toward Cys over Hcy and GSH was achieved with a limit of detection (LOD) down to 50 nM. Yoon's group (71) and Yang's group (72) reported two other types of ESIPT probes for Cys discrimination through a kinetically resolvable fluorescence signal. As shown in **Figure 5a**, **subpanel *ii***, upon Cys treatment, DAP-1 with two acrylates displayed a 65-fold enhancement in fluorescence intensity with a Stokes shift up to 162 nm as a result of the addition/cyclization of the ESIPT effect. The LOD was as low as 30 nM with an operational time of less than 15 min. Because of the faster reaction kinetics of the Michael addition/cyclization between the acrylic ester and Cys, superior selectivity could be achieved and further improved by the much closer pK_a of Cys to the physiological pH condition compared to that of Hcy and GSH.

By harnessing the ICT effect, Feng and colleagues (73) designed a turn-on probe, DBTC, for Hcy detection in living cells. As shown in **Figure 5a**, **subpanel *iii***, when Hcy was added, the aldehyde group of DBTC underwent a nucleophilic addition reaction. The formed ring broke the ICT effect, thus turning on the fluorescence signal with an LOD as low as 3.05 μM (73). Through substituting the anthracene with a TPA moiety, the same group reported another ICT probe, APTC. The LOD for Hcy was further lowered to 21.98 nM, with a reaction time of <5 min. More importantly, the excellent biocompatibility allowed APTC to image Hcy in living HeLa cells (74).

7.2. Glutathione

With concentrations of 1.0–10 mM, GSH was the most abundant biothiol in cytosol. It is of critical importance in antioxidants that regulate the intracellular buffering system. By scavenging the ROS and free radicals, GSH prevents cells from oxidative stress and toxins (75).

Tang's group (76) designed a malonitrile-functionalized TPE derivative (TPE-DCV) for GSH recognition through a thiol-ene click reaction. The sensing range was as wide as 300 μM. Owing to its excellent biocompatibility, fluorescence mapping of intracellular GSH distribution was realized (76). Based on an AIE-active polymer, Chen and coworkers (77) reported on a polymeric probe they created. It comprised disulfide-functionalized hyperbranched poly (amido-amine)s (ssHPAs) as the hydrophilic matrix, TPE as the hydrophobic unit, and a disulfide bond as the reactive linkage. The hydrophobic TPEs were randomly grafted onto the skeletons of ssHPAs, whose cavities provided isolated spaces to facilitate the intramolecular rotation of TPE units. Upon reacting with GSH, a bright fluorescence signal appeared as the cleavage of disulfide bonds destroyed the dendritic structure of TPE-ssHPAs that led to the aggregation of TPE units. A linear detection range from 2 to 100 mM with an LOD of 0.55 mM could be achieved (77).

Alternatively, Tian's group (78) presented a diselenide-containing probe for intracellular GSH sensing. As shown in **Figure 5b**, with a diselenide bond linking to the AIEgen, diselenide-containing 9,10-distyrylanthracene derivative (SeDSA) was generated, which could further self-assemble into nanoparticles with enhanced fluorescence intensity in an aqueous suspension. SeDSA nanoparticles could react with GSH because of a selenium-sulfur exchange reaction. With increased nanosize and space occupancy and decreased π–π interactions, a much stronger fluorescence was emitted from the product. Compared to the disulfide bond, the strength of the diselenide bond was much weaker, leading to a higher reductive sensitivity of diselenide bond–linked probes (78).

7.3. Hydrogen Sulfide

H_2S in mammalian cells is involved in a variety of physiological processes, including the signaling pathway, angiogenesis, and neuromodulation (79). As the concentration of H_2S quickly fluctuates

in a range from a few nanomolars to submillimolars, it is desirable to perform real-time monitoring of local H_2S with high sensitivity and selectivity (80, 81).

Taking azido ($-N_3$) as a reaction center, Kumar and colleagues (82) reported a hexaphenylbenzene-based AIE probe for H_2S imaging in living cancer cells. H_2S could then be detected with an LOD down to 0.33 mM. By introducing an electron-accepting azido group, Liu's group (83) reported an α-cyanostilbene-based probe. **Figure 5c**, **subpanel *i*** illustrates that the azido group could be rapidly reduced to the electron-donating NH_2 group in the presence of H_2S, with enormous fluorescence spectra shifting from orange to green, indicating a robust ratiometric signal for H_2S sensing in living cells.

Through the nucleophilic reaction with an indolium group, an H_2S probe, Indo-TPE-Indo, was reported by Wang's group (84). The probe can selectively recognize HS^- in mitochondria via a nucleophilic reaction, accompanied by a significant decrease in fluorescence signal in the tumor-bearing mice (84) (**Figure 5c**, **subpanel *ii***). In addition, 2,4-dinitrobenzenesulfonate ester was unitized as a reactive site for H_2S sensing. **Figure 5c**, **subpanel *iii*** shows that the AIEgens were first transferred to AIE dots in the presence of amphiphilic block copolymers. The fluorescence signal was efficiently quenched by the PET effect. Upon reacting with H_2S, the probes could be specifically cleaved with the release of hydroxy-containing fluorophores. The PET effect was thus destroyed with a strongly emitted fluorescence signal, leading to high sensitivity (43.8 nM LOD) in the real-time visualization of lysosomal H_2S (85).

By introducing nitro groups, Zeng and coworkers (86) reported an AIE/ESIPT-based nanoprobe for H_2S detection. As illustrated in **Figure 5d**, the ESIPT could be specifically initiated to turn on the fluorescence when the 2,4-dinitrophenyl ether moiety was cleaved by H_2S. The detection limit for H_2S was down to 90 μM with an operational time of less than 5 min. Furthermore, specific H_2S imaging was realized in zebrafish larvae, owing to its excellent biocompatibility and penetrability from Tat peptide modification (86).

8. SENSING OF REACTIVE OXYGEN SPECIES, REACTIVE NITROGEN SPECIES, AND RADICALS

ROS, reactive nitrogen species (RNS), and free radicals have continuously existed in biological systems. Many diseases like cancer, diabetes, and neurodegeneration develop as the result of the toxic effects of these molecules (3).

8.1. Superoxide Anion

The superoxide anion $O_2^{\cdot-}$ is a precursor of other ROS such as the hydroxyl radical ($^{\cdot}OH$) and hydrogen peroxide (H_2O_2). It plays a crucial role in regulating the signaling processes at very low concentrations. Superfluous accumulation of $O_2^{\cdot-}$ may damage membranes, tissues, and various organisms (87).

Hua and coworkers (88) reported a NIR probe, BDP, for the selective detection of $O_2^{\cdot-}$ in living cells. Alkoxy-substituted TPA and dibenzo[*a,c*]-phenazine units were introduced to obtain NIR emission and AIE properties (**Figure 6a**). The diphenyl-phosphinyl group in the probe could react with the $O_2^{\cdot-}$, resulting in the decomposition of this species. As a result, NIR emission at 716 nm was generated from the product, with an LOD as low as 70.5 nM and a Stokes shift up to 216 nm (88). Furthermore, a probe with simultaneous turn-on fluorescence/chemiluminescence signals was developed using imidazopyrazinone as the reactive motif and TPE as the fluorescence-/chemiluminescence-enhancing skeleton. The probe turned out to be highly sensitive to $O_2^{\cdot-}$ with an LOD of 0.21 nM for the fluorescence signal and 0.38 nM for the chemiluminescence signal.

a

b

c

d

FL imaging   CL imaging   CL imaging

(*Caption appears on following page*)

Figure 6 (*Figure appears on preceding page*)

Radical sensing in living systems. (*a*) Recognition mechanism for the transformation of BDP to BD by superoxide anions and the relative fluorescence intensity of BD to BDP incubated with different concentrations of KO_2 with the photograph under a UV lamp. Panel adapted with permission from Reference 88; copyright 2018 Royal Society of Chemistry. (*b*) Preparation of IRTP NPs and the $ONOO^-$ or ClO^- sensing mechanism by breaking the FRET effect between AIEgen (TBD-PEG) and IR786S. Panel adapted with permission from Reference 93; copyright 2018 American Chemical Society. (*c*) Scheme for ratiometric detection of ClO^- by an AIE-based nanoprobe and the fluorescence spectra of the nanoprobe in the presence of different concentrations of ClO^-. Panel adapted with permission from Reference 99; copyright 2016 Royal Society of Chemistry. (*d, top*) Scheme for dual-mode chemo-fluoro-luminophore QM-B-CF for H_2O_2 imaging. (*d, bottom*) In vivo CL imaging of xenograft tumor-bearing mice after intratumor injection of QM-B-CF (*top, middle*, with or without irradiation) and injection of luminol (*bottom*) as well as in vivo CL and fluorescence FL imaging of xenograft tumor-bearing mice after injection of QM-B-CF with or without NAC (*N*-acetylcysteine, H_2O_2 scavenger). Panel adapted with permission from Reference 109; copyright 2020 Wiley-VCH Verlag. Abbreviations: AIEgen, aggregation-induced emission luminogen; BD, 4-methoxy-*N*-(4-methoxyphenyl)-*N*-(4-(13-(pyridin-4-yl)dibenzo[*a,c*]phenazin-10-yl)phenyl)aniline; BDP, diphenyl-phosphinyl group–modified BD; CL, chemiluminescence; ClO^-, hypochlorous acid; FL, fluorescence; IRTP NPs, IR786S and TBD-PEG composed nanoparticles; KO_2, potassium superoxide; $ONOO^-$, peroxynitrite; PEG, polyethylene glycol; UV, ultraviolet.

Endogenous $O_2{}^{\cdot-}$ in HL-7702 cells induced by acetaminophen was continuously monitored for 7,200 s with chemiluminescence signals, and the results were confirmed by fluorescence imaging, suggesting its use as a reliable tool for real-time monitoring of endogenous $O_2{}^{\cdot-}$ in living cells (89).

8.2. Reactive Nitrogen Species

RNS comprise a class of chemically reactive species essential for many biological functions. As a prototypical RNS, nitric oxide (NO) serves as an important signaling molecule. Dysregulation of NO production is associated with various diseases (90). Tian's group (91) reported a silica nanoprobe based on AIE-active TPE-2NH2 for ratiometric NO detection in vitro. The fluorescence signal of the silica nanoparticles changed from green to red upon the reaction of NO with the *o*-phenylenediamine group in TPE-2NH2, resulting in the change in the ICT process. It exhibited very high sensitivity and selectivity to NO, with a response time of <5 min (91).

Another RNS species, peroxynitrite ($OONO^-$), is produced via the combination of nitric oxide (·NO) and $O_2{}^{\cdot-}$. Tang and colleagues (92) designed a light-up nanoprobe based on a phenylboronate TPE derivative, TPE-IPB, for the specific detection of in vivo $ONOO^-$. Nanoprobes formulated by a TPE-IPB and lipid-PEG matrix, TPE-IPB-PEG, were nonemissive in aqueous solution. However, its emission was switched on in the inflammatory region with elevated $ONOO^-$. The high specificity of the nanoprobe toward $ONOO^-$ enabled the precise and noninvasive screening of potential anti-inflammatory agents (92). Through the self-assembly of an $ONOO^-$ responsive dye IR786S and an amphiphilic polymer TBD-PEG containing AIE photosensitizers, Liu's group (93) reported a triggerable $ONOO^-$ sensing system. As shown in **Figure 6*b***, within the nanoparticles, IR786S quenched both the fluorescence signal and singlet oxygen generation of TBD due to the efficient FRET between them. Once the nanoparticles reached bacterial infection sites, IR786S was decomposed by the overexpressed $ONOO^-$, resulting in lit-up fluorescence signals from TBD (93).

8.3. Hypochlorous Acid

Among ROS, hypochlorous acid (ClO^-) is generated during phagocytosis and serves as a pathogen killer within the immune system (94). The reaction between Cl^- and H_2O_2 generates ClO^-. Excessive ClO^- can lead to inflammation-associated tissue damage and a variety of diseases (95).

Through the oxidation of thioether, Qu's group (96) designed a probe, PTZ-BT, for ClO⁻ detection. In the presence of ClO⁻, the sulfur atom in the phenothiazine group in PTZ-BT was oxidized to sulfoxide, resulting in a turn-off fluorescence response with an LOD up to 0.64 μM. The turn-off manner was improved by Zhang and colleagues (97) with a turn-on probe by taking advantage of the quenching effect from the PET process. The specific reaction between the thione unit and ClO⁻ reduced the PET effect and turned on the AIE fluorescence signal. The LOD was significantly improved to 92 nM with a detection process of <40 s.

Harnessing the oxidation of the C=C bond, Wang's group (98) developed a fluorescence colorimetry–composed dual-modality probe based on a pyrene derivative appended by 2-thioxo-dihydro-pyrimidine-4,6-dione (Py-Pd). Upon treatment with ClO⁻, cleavage of the C=C bridge led to the transformation of Py-Pd to pyrene-2-carbaldehyde (Py-CHO). The ICT effect was thus inhibited with robust fluorescence emission together with the shift in solution color from red to colorless. Sensitivity with an LOD as low as 75 nM and response time as fast as 30 s was demonstrated (98). Using a double bond in dicyanovinyl as a recognition group, Wu and coworkers (99) independently reported probes for imaging endogenous ClO⁻. ClO⁻ caused the structural transition from dicyanovinyl TPE to aldehyde TPE, thereby leading to the ratiometric fluorescence signals (100) (**Figure 6c**).

Oxidation of the Schiff base is another technique used for ClO⁻ detection. Cao's group (101) developed an AIE probe with a pyrene Schiff's base derivative. Upon nucleophilic addition and hydrolysis, a turn-on fluorescence signal could be observed with an LOD as low as 5.7 nM. Taking advantage of the AIE and ESIPT effects, Yan's group (102) reported using a salicylaldehyde Schiff's base molecule for turn-on ClO⁻ detection with ClO⁻ complexation to initiate the ESIPT effect.

Sun's group (103) designed a powerful probe for HClO imaging in living cells by combining AIE and TBET with traditional fluorophores as ClO⁻ recognition sites. The probe consists of TPE and rhodamine B thiohydrazide, acting as the dark donor and acceptor, respectively. In the absence of HClO, the aggregated probes showed a robust blue fluorescence from TPE. After reacting with HClO, the rhodamine moiety became positively charged, resulting in enhanced solubility. Thus, emission from rhodamine was recovered due to the efficient dark TBET process. More than a 7,000-fold enhancement in fluorescence signal and ultrahigh sensitivity were achieved in HClO, with an LOD up to 1.29 nM (103).

8.4. Hydrogen Peroxide

H_2O_2 is prevalent in biological systems. Abnormal levels of H_2O_2 can cause long-term damage to tissues and lead to neurodegeneration, oxidative stress, and cancer (104).

Boronate presents unique selectivity toward H_2O_2, with the aryl derivative bound to the boron atom converting to phenol (105). Lee's group (106) reported a sensitive boronated probe, triphenylimidazoleoxadiazolephenyl boronate, for H_2O_2 recognition. The nucleophilic addition of H_2O_2 to the boron generated a charged tetrahedral boronate complex following the migration of the C–B bond toward one of the electrophilic peroxide oxygen atoms. After hydrolyzation into a phenol, significant enhancements in fluorescence signal appeared because of the reduced solubility. The detection could be finished in 2 min with an LOD lowered to 8.0 nM. Moreover, more than a 1,000-fold-higher selectivity was achieved compared to in other ROS, enabling the accurate visualization of H_2O_2 in cancer cells (106). Inspired by the peroxidase-catalyzed reaction in inflammatory cells, Xia and coworkers (107) constructed an H_2O_2 probe with TPE modified by two tyrosine moieties. Owing to the H_2O_2-dependent enzymatic dimerization, tyrosine-containing TPE molecules cross-linked to form hydrophobic aggregates. The resulting turn-on fluorescence signal provided in situ information of the intracellular H_2O_2.

H$_2$O$_2$-triggered chemiluminescence is another approach for in vivo H$_2$O$_2$ tracking (108). Recently, Guo's group (109) reported a dual-lock AIE probe for H$_2$O$_2$ imaging with real-time fluorescence and a sensitive chemiluminescence signal. With an aryl boronate moiety as the recognition unit, QM-B-CF was employed for H$_2$O$_2$ sensing (**Figure 6d**). The hydrolyzation of the boronate ester group in QM-B-CF could induce the aggregation of a QM-O-CF product, along with a robust fluorescence signal and more than a 320-fold enhancement in chemiluminescence signal. Robust fluorescence and chemiluminescence signals could be observed in the tumor site after 2 h postinjection when using xenograft 4T1 tumor mouse as an in vivo model for H$_2$O$_2$ imaging. In contrast, much weaker fluorescence and chemiluminescence signals appeared in the H$_2$O$_2$ scavenger *N*-acetylcysteine-pretreated groups. Furthermore, the chemiluminescence intensity of QM-B-CF was around 66-fold higher than that of traditional luminol, showing an accurate sensing platform for in vivo physiological dynamics (109).

9. CONCLUSION AND PERSPECTIVE

AIE-derived small molecules, polymers, and nanomaterials have shown unique optical properties that are valuable for powerful applications in visualization and imaging of critical physiological dynamics in living systems. AIE technologies overcome the shortcomings of traditional organic fluorophores and inorganic nanomaterials, including severe photobleaching, moderate signal-to-noise ratio, the ACQ effect, and potential toxicity. Moreover, various novel AIE systems have recently arisen, leading to unprecedented and exciting advancements in optical properties, including long emission wavelength, extended luminescence lifetime (110, 111), multiexcitable (from photo-, electro-, and tribo- to target-stimulated chemo- and bio-) luminescence, and smart responsiveness with artificial intelligence.

Two prospective areas are still in their early stages and need more exploration. Increasing evidence suggests that mechanical forces are critical in regulating physiology and diseases. For example, forces play important roles in stem cell differentiation and in organized germ layer patterning in mammalian embryogenesis (112). Mechanical forces also participate extensively in cancer progression (113). However, quantification of mechanical forces generated by living cells and tissues is still far from satisfactory using traditional methods that suffer from limited biointerface ability and moderate sensitivity to tiny biomechanical changes. Based on the rapid progress in triboluminescence (111), AIE probes applied to biomechanical sensing and imaging are promising in their excellent biocompatibilities, ultrahigh sensitivities, and rapid responsiveness. In addition, monitoring neuronal activities has long been desired to understand the mysterious function of the brain and the underlying mechanisms of neurological disorders such as Alzheimer's disease (114). In that respect, the potassium ion (K$^+$) is a key determinant of membrane potential and has been regarded as a main target of investigation (115). Owing to the success of AIE-based ionic sensors in versatile sensing applications (116, 117), AIE technologies have the potential to succeed in neuronal activity mapping and finally deciphering mysteries of the brain.

As each system has its own pros and cons, there are still many hurdles to overcome to promote the effective use of AIEgens in physiological dynamic monitoring and visualization. The first problem involves targeting selectivity. This may cause restrictions in the differentiation of various subtypes of physiological items, especially when confronting intercrosslinked factors, such as viscosity and polarity, redox state, and ROS/radical level. However, with the rapid developments of AIEgens, we believe some specific candidates could be designed and selected from a variety of compounds. Furthermore, after conjugation with canonic targeting moieties, such as pH-responsible aptamers, monoclonal antibodies that can guide an AIEgen to the intracellular local site to target

certain parameters, a promising step would be to endow the resulting fluorescent AIEgen with specific targeting properties that could respond to a certain type of physiological dynamic.

Another challenge involves the sensitivity and accuracy of the AIEgens in physiological dynamic monitoring. The dynamic processes in living cells and animals normally fluctuate in a very narrow spectrum and range, and a tiny change in physiological activity can have significant effects. Moreover, biological processes such as membrane potential dynamics can change rapidly. These require the AIE probes to respond sensitively in both spatial and temporal dimensions. Because the sensing procedures of AIEgens with physiological dynamics normally depend on the efficiency and rapidness of the reactions between them, it would be possible to select some reaction-based systems that could meet these sensitivity requirements. Moreover, sensing precision must also be considered. The complicated physiological environments in living cells and bodies mean the AIE probes may simultaneously encounter thousands of stimuli, especially intercrosslinked parameters. Second sets of signals to confirm multimodality sensing and imaging, such as fluorescence intensity/wavelength (emission color)/lifetime and colorimetry, surface-plasmonic resonance, or Raman, with distinct but complementary signals when they interreact with the same target, would be helpful to enhance precision and eliminate false positives to a large extent.

The final challenge to overcome involves biocompatibility when using AIEgens in biosystems. Because physiological dynamics originate from their natural growth, metabolism, differentiation, propagation, aging, or apoptosis, the AIEgens should not disturb these bioactivities or introduce extra stress to living systems. Otherwise, it will be very hard to determine whether the produced signal comes from the inherent physiological dynamics.

Additional attention should be focused on the practicability and clinical translation of AIEgens. For basic laboratory research, fluorescence imaging has unique advantages for in situ visualization of biotargets at the molecular level and monitoring of dynamic bioprocesses in real time to discern their distinctive sensitivity, rapidness, convenience, and spatial-temporal resolution. As superior alternatives for light-up fluorescence imaging, AIEgens display significant improvements in photobleaching resistance and biocompatibility compared to the traditional and commercially available organic dyes and inorganic nanoparticles. AIE-based materials have already been widely applied in chemo-/bioanalyte analysis, subcellular or cellular imaging, tissue/organ visualization, and whole-body monitoring. Importantly, AIEgens also demonstrate great potential for investigating complex bioprocesses, such as drug delivery, siRNA/gene interference, bacteriophage infection, and tumor tracking. Various types of AIE products, such as G-quadruplex detection, glucose/pH sensing, and mitochondria/cardiolipin probing, are now commercially available for laboratory research and show much improved properties than do existing reagents on the market (e.g., see products from AIEgen Biotech, **http://www.aiegen.com.hk/**).

In the in vitro detection market, the strip-based system represents one of the most convenient point-of-care products for signal readout in daily life. Although it is difficult to integrate AIEgens into strip-tests for point-of-care products, owing to the natural turn-on fluorescence after they aggregate in the strip matrix, it would be possible to develop a solution-based system for an analyte assay. A good example is the virus immunoassay coupled with antibody-mediated enzyme-linked immunosorbent assay (ELISA) and magnetic enzyme-linked immunoassay in the plate via reaction in solution (18). In addition, with the development and growth of engineering methods, especially the rapid advancement in nanotechnological strategies, it would also be promising to manipulate AIEgens in the strip matrix to achieve fluorescent signal change. For clinical applications in vivo for human health, the most important issue is biosafety, which must be thoroughly investigated in the fields of pharmaceuticals, pharmacology, clinical pharmacokinetics, and toxicology. Parameters such as blood/cell biocompatibility, colloidal stability, dosage of administration, blood circulation

time, effective concentration in the lesion, and the biodegradation half-life should all be tested and meet standards of the US Food and Drug Administration. Once these challenges have been overcome, researchers will then be equipped to generate revolutionary functionalities and make these AIE-based materials highly practicable for clinical-oriented biomedical applications.

DISCLOSURE STATEMENT

ACKNOWLEDGMENTS

LITERATURE CITED

1. Vaupel P, Schlenger K, Knoop C, Höckel M. 1991. Oxygenation of human tumors: evaluation of tissue oxygen distribution in breast cancers by computerized O_2 tension measurements. *Cancer Res*. 51:3316–22

2. Armstrong JS, Steinauer KK, Hornung B, Irish JM, Lecane P, et al. 2002. Role of glutathione depletion and reactive oxygen species generation in apoptotic signaling in a human B lymphoma cell line. *Cell Death Differ*. 9:252–63

3. D'Autréaux B, Toledano MB. 2007. ROS as signalling molecules: mechanisms that generate specificity in ROS homeostasis. *Nat. Rev. Mol. Cell Biol*. 8:813–24

4. Lusic H, Grinstaff MW. 2012. X-ray-computed tomography contrast agents. *Chem. Rev.* 113:1641–66

5. Fan W, Yung B, Huang P, Chen X. 2017. Nanotechnology for multimodal synergistic cancer therapy. *Chem. Rev.* 117:13566–638

6. He X, Ma N. 2014. An overview of recent advances in quantum dots for biomedical applications. *Colloid. Surf. B Biointerfaces* 124:118–31

7. He X, Xiong L-H, Zhao Z, Wang Z, Luo L, et al. 2019. AIE-based theranostic systems for detection and killing of pathogens. *Theranostics* 9:3223–48

8. Liu H, Xiong L-H, Kwok RTK, He X, Lam JWY, et al. 2020. AIE bioconjugates for biomedical applications. *Adv. Opt. Mater*. 8:2000162

9. Kobayashi H, Ogawa M, Alford R, Choyke PL, Urano Y. 2009. New strategies for fluorescent probe design in medical diagnostic imaging. *Chem. Rev.* 110:2620–40

10. He X, Zeng T, Li Z, Wang G, Ma N. 2016. Catalytic molecular imaging of microRNA in living cells by DNA-programmed nanoparticle disassembly. *Angew. Chem. Int. Ed.* 55:3073–76

11. Wei W, He X, Ma N. 2014. DNA-templated assembly of a heterobivalent quantum dot nanoprobe for extra- and intracellular dual-targeting and imaging of live cancer cells. *Angew. Chem. Int. Ed.* 53:5573–77

12. Li Z, He X, Luo X, Wang L, Ma N. 2016. DNA-programmed quantum dot polymerization for ultra-sensitive molecular imaging of cancer cells. *Anal. Chem.* 88:9355–58

13. Yong K-T, Law W-C, Hu R, Ye L, Liu L, et al. 2013. Nanotoxicity assessment of quantum dots: from cellular to primate studies. *Chem. Soc. Rev.* 42:1236–50

14. He X, Li Z, Chen M, Ma N. 2014. DNA-programmed dynamic assembly of quantum dots for molecular computation. *Angew. Chem. Int. Ed.* 53:14447–50

15. Mei J, Leung NLC, Kwok RTK, Lam JWY, Tang BZ. 2015. Aggregation-induced emission: together we shine, united we soar! *Chem. Rev.* 115:11718–940

16. Kwok RTK, Leung CWT, Lam JWY, Tang BZ. 2015. Biosensing by luminogens with aggregation-induced emission characteristics. *Chem. Soc. Rev.* 44:4228–38

17. Gao Y, He Z, He X, Zhang H, Weng J, et al. 2019. Dual-color emissive AIEgen for specific and label-free double-stranded DNA recognition and single-nucleotide polymorphisms detection. *J. Am. Chem. Soc.* 141:20097–106

18. Xiong L-H, He X, Zhao Z, Kwok RTK, Xiong Y, et al. 2018. Ultrasensitive virion immunoassay platform with dual-modality based on a multifunctional aggregation-induced emission luminogen. *ACS Nano* 12:9549–57

19. Niu G, Zheng X, Zhao Z, Zhang H, Wang J, et al. 2019. AIE-active functionalized acrylonitriles: structure tuning by simple reaction-condition variation, efficient red emission and two-photon bioimaging. *J. Am. Chem. Soc.* 141:15111–20

20. He X, Zhao Z, Xiong L-H, Gao PF, Peng C, et al. 2018. Redox-active AIEgen-derived plasmonic and fluorescent core@shell nanoparticles for multimodality bioimaging. *J. Am. Chem. Soc.* 140:6904–11

21. Qin W, Alifu N, Cai Y, Lam JWY, He X, et al. 2019. Synthesis of an efficient far-red/near-infrared luminogen with AIE characteristics for in vivo bioimaging applications. *Chem. Commun.* 55:5615–18

22. He X, Xiong L-H, Huang Y, Zhao Z, Wang Z, et al. 2020. AIE-based energy transfer systems for biosensing, imaging, and therapeutics. *TrAC Trends Anal. Chem.* 122:115743

23. Wang Y, Zhang Y, Wang J, Liang X-J. 2019. Aggregation-induced emission (AIE) fluorophores as imaging tools to trace the biological fate of nano-based drug delivery systems. *Adv. Drug Deliv. Rev.* 143:161–76

24. He X, Yin F, Wang D, Xiong L-H, Kwok RTK, et al. 2019. AIE featured inorganic-organic core@shell nanoparticle for high-efficiency siRNA delivery and real-time monitoring. *Nano Lett.* 19:2272–79

25. Cheng Y, Sun C, Liu R, Yang J, Dai J, et al. 2019. A multifunctional peptide-conjugated AIEgen for efficient and sequential targeted gene delivery into the nucleus. *Angew. Chem. Int. Ed.* 58:5049–53

26. He X, Yang Y, Guo Y, Lu S, Du Y, et al. 2020. Phage-guided targeting, discriminative imaging, and synergistic killing of bacteria by AIE bioconjugates. *J. Am. Chem. Soc.* 142:3959–69

27. Gao Y, Wang X, He X, He Z, Yang X, et al. 2019. A dual-functional photosensitizer for ultraefficient photodynamic therapy and synchronous anticancer efficacy monitoring. *Adv. Funct. Mater.* 29:1902673

28. He X, Peng C, Qiang S, Xiong L-H, Zhao Z, et al. 2020. Less is more: silver-AIE core@shell nanoparticles for multimodality cancer imaging and synergistic therapy. *Biomaterials* 238:119834

29. Casey JR, Grinstein S, Orlowski J. 2010. Sensors and regulators of intracellular pH. *Nat. Rev. Mol. Cell Biol.* 11:50–61

30. Srivastava J, Barber DL, Jacobson MP. 2007. Intracellular pH sensors: design principles and functional significance. *Physiology* 22:30–39

31. Chen S, Hong Y, Liu Y, Liu J, Leung CWT, et al. 2013. Full-range intracellular pH sensing by an aggregation-induced emission-active two-channel ratiometric fluorogen. *J. Am. Chem. Soc.* 135:4926–29

32. Chao J, Wang H, Zhang Y, Yin C, Huo F, et al. 2018. A novel pyrene-based dual multifunctional fluorescent probe for differential sensing of pH and HSO_3^- and their bioimaging in live cells. *New J. Chem.* 42:3322–33

33. Yin H, Zhao B, Kan W, Ding L, Wang L, et al. 2020. A phenanthro[9, 10-*d*]imidazole-based optical sensor for dual-responsive turn-on detection of acidic pH and Cu^{2+} in chicken blood and living cells. *Dyes Pigm.* 173:107916

34. Song P, Chen X, Xiang Y, Huang L, Zhou Z, et al. 2011. A ratiometric fluorescent pH probe based on aggregation-induced emission enhancement and its application in live-cell imaging. *J. Mater. Chem.* 21:13470–75

35. Bai Y, Liu D, Han Z, Chen Y, Chen Z, et al. 2018. BODIPY-derived ratiometric fluorescent sensors: pH-regulated aggregation-induced emission and imaging application in cellular acidification triggered by crystalline silica exposure. *Sci. China Chem.* 61:1413–22

36. Yu Y, Yu C, Wu Q, Wang H, Jiao L, et al. 2019. Pure *E/Z* isomers of *N*-methylpyrrole-benzohydrazide-based BF_2 complexes: remarkable aggregation-, crystallization-induced emission switching properties and application in sensing intracellular pH microenvironment. *J. Mater. Chem. C* 7:4533–42

37. Dou Y, Kenry Liu J, Zhang F, Cai C, et al. 2019. 2-Styrylquinoline-based two-photon AIEgens for dual monitoring of pH and viscosity in living cells. *J. Mater. Chem. B* 7:7771–75

38. Li K, Feng Q, Niu G, Zhang W, Li Y, et al. 2018. Benzothiazole-based AIEgen with tunable excited-state intramolecular proton transfer and restricted intramolecular rotation processes for highly sensitive physiological pH sensing. *ACS Sens.* 3:920–28

39. Zhao X, Chen Y, Niu G, Gu D, Wang J, et al. 2019. Photostable pH-sensitive near-infrared aggregation-induced emission luminogen for long-term mitochondrial tracking. *ACS Appl. Mater. Interfaces* 11:13134–39

40. Lin N, Chen X, Yan S, Wang H, Lu Z, et al. 2016. An aggregation-induced emission-based pH-sensitive fluorescent probe for intracellular acidity sensing. *RSC Adv.* 6:25416–19

41. Shi X, Yan N, Niu G, Sung SHP, Liu Z, et al. 2020. In vivo monitoring of tissue regeneration using a ratiometric lysosomal AIE probe. *Chem. Sci.* 11:3152–63

42. Qiu J, Jiang S, Guo H, Yang F. 2018. An AIE and FRET-based BODIPY sensor with large stoke shift: novel pH probe exhibiting application in CO_3^{2-} detection and living cell imaging. *Dyes Pigm.* 157:351–58

43. Fang M, Xia S, Bi J, Wigstrom TP, Valenzano L, et al. 2018. A cyanine-based fluorescent cassette with aggregation-induced emission for sensitive detection of pH changes in live cells. *Chem. Commun.* 54:1133–36

44. Wang J, Xia S, Bi J, Fang M, Mazi W, et al. 2018. Ratiometric near-infrared fluorescent probes based on through-bond energy transfer and π-conjugation modulation between tetraphenylethene and hemicyanine moieties for sensitive detection of pH changes in live cells. *Bioconjug. Chem.* 29:1406–18

45. Qi Q, Li Y, Yan X, Zhang F, Jiang S, et al. 2016. Intracellular pH sensing using polymeric micelle containing tetraphenylethylene-oxazolidine. *Polym. Chem.* 7:5273–80

46. Hu Y, Han T, Yan N, Liu J, Liu X, et al. 2019. Visualization of biogenic amines and in vivo ratiometric mapping of intestinal pH by AIE-active polyheterocycles synthesized by metal-free multicomponent polymerizations. *Adv. Funct. Mater.* 29:1902240

47. Lowell BB, Spiegelman BM. 2000. Towards a molecular understanding of adaptive thermogenesis. *Nature* 404:652–60

48. Gao H, Kam C, Chou TY, Wu M-Y, Zhao X, et al. 2020. A simple yet effective AIE-based fluorescent nano-thermometer for temperature mapping in living cells using fluorescence lifetime imaging microscopy. *Nanoscale Horiz.* 5:488–94

49. Wang Z, He X, Yong T, Miao Y, Zhang C, et al. 2020. Multicolor tunable polymeric nanoparticle from the tetraphenylethylene cage for temperature sensing in living cells. *J. Am. Chem. Soc.* 142:512–19

50. Luby-Phelps K. 1999. Cytoarchitecture and physical properties of cytoplasm: volume, viscosity, diffusion, intracellular surface area. *Int. Rev. Cytol.* 192:189–221

51. Mecocci P, Beal MF, Cecchetti R, Polidori MC, Cherubini A, et al. 1997. Mitochondrial membrane fluidity and oxidative damage to mitochondrial DNA in aged and AD human brain. *Mol. Chem. Neuropathol.* 31:53–64

52. Chen S, Hong Y, Zeng Y, Sun Q, Liu Y, et al. 2015. Mapping live cell viscosity with an aggregation-induced emission fluorogen by means of two-photon fluorescence lifetime imaging. *Chem. Eur. J.* 21:4315–20

53. Chen W, Gao C, Liu X, Liu F, Wang F, et al. 2018. Engineering organelle-specific molecular viscosimeters using aggregation-induced emission luminogens for live cell imaging. *Anal. Chem.* 90:8736–41

54. Wodarz A, Näthke I. 2007. Cell polarity in development and cancer. *Nat. Cell Biol.* 9:1016–24

55. Owyong TC, Subedi P, Deng J, Hinde E, Paxman JJ, et al. 2020. A molecular chameleon for mapping subcellular polarity in an unfolded proteome environment. *Angew. Chem. Int. Ed.* 59:10129–35

56. Gandre-Babbe S, van der Bliek AM. 2008. The novel tail-anchored membrane protein Mff controls mitochondrial and peroxisomal fission in mammalian cells. *Mol. Biol. Cell* 19:2402–12

57. Ow Y-LP, Green DR, Hao Z, Mak TW. 2008. Cytochrome *c*: functions beyond respiration. *Nat. Rev. Mol. Cell Biol.* 9:532–42

58. Li J, Kwon N, Jeong Y, Lee S, Kim G, et al. 2017. Aggregation-induced fluorescence probe for monitoring membrane potential changes in mitochondria. *ACS Appl. Mater. Interfaces* 10:12150–54

59. Zhao N, Chen S, Hong Y, Tang BZ. 2015. A red emitting mitochondria-targeted AIE probe as an indicator for membrane potential and mouse sperm activity. *Chem. Commun.* 51:13599–602

60. Zhang L, Liu W, Huang X, Zhang G, Wang X, et al. 2015. Old is new again: a chemical probe for targeting mitochondria and monitoring mitochondrial membrane potential in cells. *Analyst* 140:5849–54

61. Zeng Z, Ren X, Yin T, Gao X, Tsai M, et al. 2019. Multiplexed detection and the establishment of a novel high-throughput method for human germ cell quality screening based on aggregation-induced emission. *Am. J. Transl. Res.* 11:6907

62. Situ B, Chen S, Zhao E, Leung CWT, Chen Y, et al. 2016. Real-time imaging of cell behaviors in living organisms by a mitochondria-targeting AIE fluorogen. *Adv. Funct. Mater.* 26:7132–38

63. Xue T, Jia X, Wang J, Xiang J, Wang W, et al. 2019. "Turn-on" activatable AIE dots for tumor hypoxia imaging. *Chem. Eur. J.* 25:9634–38

64. Xue T, Shao K, Xiang J, Pan X, Zhu Z, et al. 2020. In situ construction of a self-assembled AIE probe for tumor hypoxia imaging. *Nanoscale* 12:7509–13

65. Xu C, Zou H, Zhao Z, Zhang P, Kwok RT, et al. 2019. A new strategy toward "simple" water-soluble AIE probes for hypoxia detection. *Adv. Funct. Mater.* 29:1903278

66. You X, Li L, Li X, Ma H, Zhang G, et al. 2016. A new tetraphenylethylene-derived fluorescent probe for nitroreductase detection and hypoxic-tumor-cell imaging. *Chem. Asian J.* 11:2918–23

67. Lin Y, Sun L, Zeng F, Wu S. 2019. An unsymmetrical squaraine-based activatable probe for imaging lymphatic metastasis by responding to tumor hypoxia with MSOT and aggregation-enhanced fluorescent imaging. *Chem. Eur. J.* 25:16740–47

68. Weerapana E, Wang C, Simon GM, Richter F, Khare S, et al. 2010. Quantitative reactivity profiling predicts functional cysteines in proteomes. *Nature* 468:790–95

69. Liu Y, Yu Y, Lam JW, Hong Y, Faisal M, et al. 2010. Simple biosensor with high selectivity and sensitivity: thiol-specific biomolecular probing and intracellular imaging by AIE fluorogen on a TLC plate through a thiol–ene click mechanism. *Chem. Eur. J.* 16:8433–38

70. Zhou X, Guo D, Jiang Y, Gong D-M, Zhao X-J, et al. 2017. A novel AIEE and ESIPT fluorescent probe for selective detection of cysteine. *Tetrahedron Lett.* 58:3214–18

71. Cui L, Baek Y, Lee S, Kwon N, Yoon J. 2016. An AIE and ESIPT based kinetically resolved fluorescent probe for biothiols. *J. Mater. Chem. C* 4:2909–14

72. Sheng H, Hu Y, Zhou Y, Fan S, Cao Y, et al. 2018. A hydroxyphenylquinazolinone-based fluorescent probe for turn-on detection of cysteine with a large Stokes shift and its application in living cells. *J. Photochem. Photobiol. A* 364:750–57

73. Chu Y, Xie Z, Yue Y, Yue Y, Kong X, et al. 2019. New fast, highly selective probe with both aggregation-induced emission enhancement and intramolecular charge-transfer characteristics for homocysteine detection. *ACS Omega* 4:5367–73

74. Chu Y, Xie Z, Zhuang D, Yue Y, Yue Y, et al. 2019. An intramolecular charge transfer and aggregation induced emission enhancement fluorescent probe based on 2-phenyl-1,2,3-triazole for highly selective and sensitive detection of homocysteine and its application in living cells. *Chin. J. Chem.* 37:1216–22

75. Townsend DM, Tew KD, Tapiero H. 2003. The importance of glutathione in human disease. *Biomed. Pharmacother.* 57:145–55

76. Lou X, Hong Y, Chen S, Leung CWT, Zhao N, et al. 2014. A selective glutathione probe based on AIE fluorogen and its application in enzymatic activity assay. *Sci. Rep.* 4:4272

77. Wang B, Li C, Yang L, Zhang C, Liu L-J, et al. 2019. Tetraphenylethene decorated with disulfide-functionalized hyperbranched poly (amido amine)s as metal/organic solvent-free turn-on AIE probes for biothiol determination. *J. Mater. Chem. B* 7:3846–55

78. Han W, Zhang S, Qian J, Zhang J, Wang X, et al. 2019. Redox-responsive fluorescent nanoparticles based on diselenide-containing AIEgens for cell imaging and selective cancer therapy. *Chem. Asian J.* 14:1745–53

79. Reiffenstein R, Hulbert WC, Roth SH. 1992. Toxicology of hydrogen sulfide. *Annu. Rev. Pharmacol. Toxicol.* 32:109–34

80. Luo Y, Zhu C, Du D, Lin Y. 2019. A review of optical probes based on nanomaterials for the detection of hydrogen sulfide in biosystems. *Anal. Chim. Acta* 106:1–12

81. Chen M, Chen R, Shi Y, Wang J, Cheng Y, et al. 2018. Malonitrile-functionalized tetraphenylpyrazine: aggregation-induced emission, ratiometric detection of hydrogen sulfide, and mechanochromism. *Adv. Funct. Mater.* 28:1704689

82. Pramanik S, Bhalla V, Kim HM, Singh H, Lee HW, et al. 2015. A hexaphenylbenzene based AIEE active two photon probe for the detection of hydrogen sulfide with tunable self-assembly in aqueous media and application in live cell imaging. *Chem. Commun.* 51:15570–3

83. Zhao B, Yang B, Hu X, Liu B. 2018. Two colorimetric and ratiometric fluorescence probes for hydrogen sulfide based on AIE strategy of α–cyanostilbenes. *Spectrochim. Acta A* 199:117–22

84. Ma Y, Wang H, Su S, Chen Y, Li Y, et al. 2019. A red mitochondria-targeted AIEgen for visualizing H_2S in living cells and tumours. *Analyst* 144:3381–88

85. Zhang P, Hong Y, Wang H, Yu M, Gao Y, et al. 2017. Selective visualization of endogenous hydrogen sulfide in lysosomes using aggregation induced emission dots. *Polym. Chem.* 8:7271–78

86. Zhang P, Nie X, Gao M, Zeng F, Qin A, et al. 2017. A highly selective fluorescent nanoprobe based on AIE and ESIPT for imaging hydrogen sulfide in live cells and zebrafish. *Mater. Chem. Front.* 1:838–45

87. Kontos HA, Wei EP. 1986. Superoxide production in experimental brain injury. *J. Neurosurg.* 64:803–7

88. Yang J, Liu X, Wang H, Tan H, Xie X, et al. 2018. A turn-on near-infrared fluorescence probe with aggregation-induced emission based on dibenzo[*a,c*]phenazine for detection of superoxide anions and its application in cell imaging. *Analyst* 143:1242–49

89. Niu J, Fan J, Wang X, Xiao Y, Xie X, et al. 2017. Simultaneous fluorescence and chemiluminescence turned on by aggregation-induced emission for real-time monitoring of endogenous superoxide anion in live cells. *Anal. Chem.* 89:7210–15

90. Alderton WK, Cooper CE, Knowles RG. 2001. Nitric oxide synthases: structure, function and inhibition. *Biochem. J.* 357:593–615

91. Liu L, Zhang F, Xu B, Tian W. 2017. Silica nanoparticles based on an AIE-active molecule for ratiometric detection of RNS in vitro. *J. Mater. Chem. B* 5:9197–203

92. Song Z, Mao D, Sung SH, Kwok RT, Lam JW, et al. 2016. Activatable fluorescent nanoprobe with aggregation-induced emission characteristics for selective in vivo imaging of elevated peroxynitrite generation. *Adv. Mater.* 28:7249–56

93. Wu W, Mao D, Cai X, Duan Y, Hu F, et al. 2018. ONOO⁻ and ClO⁻ responsive organic nanoparticles for specific in vivo image-guided photodynamic bacterial ablation. *Chem. Mater.* 30:3867–73

94. Davies MJ. 2010. Myeloperoxidase-derived oxidation: mechanisms of biological damage and its prevention. *J. Clin. Biochem. Nutr.* 48:8–19

95. Yadav AK, Bracher A, Doran SF, Leustik M, Squadrito GL, et al. 2010. Mechanisms and modification of chlorine-induced lung injury in animals. *Proc. Am. Thorac. Soc.* 7:278–83

96. Wang L, Chen X, Xia Q, Liu R, Qu J. 2018. Deep-red AIE-active fluorophore for hypochlorite detection and bioimaging in live cells. *Ind. Eng. Chem. Res.* 57:7735–41

97. Dong X, Zhang G, Shi J, Wang Y, Wang M, et al. 2017. A highly selective fluorescence turn-on detection of ClO⁻ with 1-methyl-1, 2-dihydropyridine-2-thione unit modified tetraphenylethylene. *Chem. Commun.* 53:11654–57

98. Gu J, Li X, Zhou Z, Liao R, Gao J, et al. 2019. Synergistic regulation of effective detection for hypochlorite based on a dual-mode probe by employing aggregation induced emission (AIE) and intramolecular charge transfer (ICT) effects. *Chem. Eng. J.* 368:157–64

99. Huang Y, Zhang P, Gao M, Zeng F, Qin A, et al. 2016. Ratiometric detection and imaging of endogenous hypochlorite in live cells and in vivo achieved by using an aggregation induced emission (AIE)-based nanoprobe. *Chem. Commun.* 52:7288–91

100. Yu H-X, Zhi J, Shen T, Ding W, Zhang X, et al. 2019. Donor–acceptor type aggregation-induced emission luminophores based on the 1,1-dicyanomethylene-3-indanone unit for bridge-dependent reversible mechanochromism and light-up biosensing of hypochlorites. *J. Mater. Chem. C* 7:8888–97

101. Zhu Y, Wang K, Wu X, Sun Y, Gong X, et al. 2020. A highly sensitive turn-on fluorescent probe for real-time detecting hypochlorite and its application in living cells. *Talanta* 209:120548

102. Xie Y, Yan L, Tang Y, Tang M, Wang S, et al. 2019. A smart fluorescent probe based on salicylaldehyde Schiff's base with AIE and ESIPT characteristics for the detections of N_2H_4 and ClO⁻. *J. Fluoresc.* 29:399–406

103. Duan Q, Zheng G, Li Z, Cheng K, Zhang J, et al. 2019. An ultra-sensitive ratiometric fluorescent probe for hypochlorous acid detection by the synergistic effect of AIE and TBET and its application of detecting exogenous/endogenous HOCl in living cells. *J. Mater. Chem. B* 7:5125–31

104. Reuter S, Gupta SC, Chaturvedi MM, Aggarwal BB. 2010. Oxidative stress, inflammation, and cancer: How are they linked? *Free Radic. Biol. Med.* 49:1603–16

105. Zhang W, Liu W, Li P, Huang F, Wang H, et al. 2015. Rapid-response fluorescent probe for hydrogen peroxide in living cells based on increased polarity of C–B bonds. *Anal. Chem.* 87:9825–28

106. Selvaraj M, Rajalakshmi K, Nam Y-S, Lee Y, Kim BC, et al. 2019. Rapid-response and highly sensitive boronate derivative-based fluorescence probe for detecting H_2O_2 in living cells. *J. Anal. Methods Chem.* 2019:5174764

107. Cheng Y, Dai J, Sun C, Liu R, Zhai T, et al. 2018. An intracellular H_2O_2-responsive AIEgen for the peroxidase-mediated selective imaging and inhibition of inflammatory cells. *Angew. Chem. Int. Ed.* 57:3123–27

108. Mao D, Wu W, Ji S, Chen C, Hu F, et al. 2017. Chemiluminescence-guided cancer therapy using a chemiexcited photosensitizer. *Chemistry* 3:991–1007

109. Zhang Y, Yan C, Wang C, Guo Z, Liu X, et al. 2020. A sequential dual-lock strategy for photoactivatable chemiluminescent probes enabling bright duplex optical imaging. *Angew. Chem. Int. Ed.* 59:9059–66

110. Xiong Y, Zhao Z, Zhao W, Ma H, Peng Q, et al. 2018. Designing efficient and ultralong pure organic room-temperature phosphorescent materials by structural isomerism. *Angew. Chem. Int. Ed.* 57:7997–8001

111. Zhang X, Du L, Zhao W, Zhao Z, Xiong Y, et al. 2019. Ultralong UV/mechano-excited room temperature phosphorescence from purely organic cluster excitons. *Nat. Commun.* 10:5161

112. Wang N. 2017. Review of cellular mechanotransduction. *J. Phys. D Appl. Phys.* 50:233002

113. Tajik A, Zhang Y, Wei F, Sun J, Jia Q, et al. 2016. Transcription upregulation via force-induced direct stretching of chromatin. *Nat. Mater.* 15:1287–96

114. Liu J, Li F, Wang Y, Pan L, Lin P, et al. 2020. A sensitive and specific nanosensor for monitoring extracellular potassium levels in the brain. *Nat. Nanotechnol.* 15:321–30

115. Liu J, Pan L, Shang C, Lu B, Wu R, et al. 2020. A highly sensitive and selective nanosensor for near-infrared potassium imaging. *Sci. Adv.* 6:eaax9757

116. Feng X, Li Y, He X, Liu H, Zhao Z, et al. 2018. A substitution-dependent light-up fluorescence probe for selectively detecting Fe^{3+} ions and its cell imaging application. *Adv. Funct. Mater.* 28:1802833

117. Gao M, Li Y, Chen X, Li S, Ren L, et al. 2018. Aggregation-induced emission probe for light-up and in situ detection of calcium ions at high concentration. *ACS Appl. Mater. Interfaces* 10:14410–17